IOPscience iopscience.iop.org

Home Search Collections Journals About Contact us My IOPscience

Ferromagnetic resonance investigation of magnetism in Fe-rich $Fe_{100-x}Ti_x$ sputtered amorphous alloys

This article has been downloaded from IOPscience. Please scroll down to see the full text article.

1997 J. Phys.: Condens. Matter 9 2085

(http://iopscience.iop.org/0953-8984/9/9/020)

View the table of contents for this issue, or go to the journal homepage for more

Download details:
IP Address: 171.66.16.207
The article was downloaded on 14/05/2010 at 08:15

Please note that terms and conditions apply.

J. Phys.: Condens. Matter **9** (1997) 2085–2107. Printed in the UK PII: S0953-8984(97)77807-X

Ferromagnetic resonance investigation of magnetism in Fe-rich $Fe_{100-x}Ti_x$ sputtered amorphous alloys

G Manjusri†, T V S M Mohan Babu†, S N Kaul† and T Lucinski‡

† School of Physics, University of Hyderabad, Central University PO, Hyderabad-500 046, India
‡ Institute of Molecular Physics, Polish Academy of Sciences 60-179 Poznán, Poland

Received 13 September 1996

Abstract. Fe-rich $Fe_{100-x}Ti_x$ alloys in the Ti concentration range $9 \leqslant x \leqslant 11$ have been successfully prepared in the *amorphous* state for the first time using the DC co-sputtering method. Exhaustive ferromagnetic resonance (FMR) measurements were performed on these alloys at a fixed microwave-field frequency of about 9.23 GHz in the temperature range 77–300 K. In this temperature range, a single resonance is observed for the alloys with $x = 10$ and 11 as against two resonances (primary and secondary), having different properties, in the case of a-$Fe_{91}Ti_9$. For the primary (single) resonance in a-$Fe_{91}Ti_9$ (the alloys with $x = 10$ and 11), the 'in-plane' uniaxial anisotropy field $H_K(T, x)$ *scales* with the saturation magnetization $M_S(T, x)$. This result suggests that the anisotropy energy is of dipolar origin. By contrast, the relation $H_K \propto M_S$ breaks down in the case of secondary resonance. The primary and secondary resonances thus characterize two distinctly different amorphous magnetic phases which widely differ in their chemical as well as geometrical short-range orders. For all the alloys in question, thermal demagnetization is mainly due to spin-wave (SW) excitations, and the SW stiffness D decreases with increasing x. SW modes soften at $T \leqslant T_{RE}$ (the so-called re-entrant transition temperature) and D possesses a reduced value for $T < T_{RE}$. The existence of a re-entrant state at low temperatures is also vindicated by the rapid increase in the magnitude of the peak-to-peak FMR linewidth ΔH_{pp} below a certain temperature. The temperature at which an upturn occurs in $\Delta H_{pp}(T)$ shifts to lower temperatures as the Fe concentration is decreased, indicating that the re-entrant behaviour is progressively suppressed with increasing x.

1. Introduction

The physical properties of amorphous (a-)Fe_{100-x} TM_x (TM = Zr, Hf or Sc) alloys with x in the range $8 \leqslant x \leqslant 12$ have been a field of intense scientific activity lately. Such overwhelming interest in these alloy systems stems from the fact that they exhibit a wide variety of novel physical phenomena such as itinerant ferromagnetism [1–5], the Invar effect [3, 6–8], re-entrant or spin-glass behaviour at low temperatures [1, 4, 5, 9–16], a broad distribution of magnetic hyperfine fields [10, 12–14, 16–23], anomalous resonant microwave absorption [24–28] and electrical resistivity minima [29–31] at temperatures close to the Curie temperature T_C. Although Ti, Zr and Hf belong to the *same* group in the periodic table, little information is at present available about the nature of magnetic ordering and transport phenomena in a-$Fe_{100-x}Ti_x$ alloys in the Ti concentration range $20 \leqslant x \leqslant 45$ ($20 \leqslant x \leqslant 45$ [32–34]). Such information (*crucial* to a complete understanding of the physical behaviour of Fe-rich amorphous alloys) about these systems could not be gathered in the past because $Fe_{100-x}Ti_x$ alloys with $x < 20$ could not be prepared [33, 34] in the amorphous state previously. We have succeeded in preparing amorphous alloys over the

0953-8984/97/092085+23$19.50 © 1997 IOP Publishing Ltd

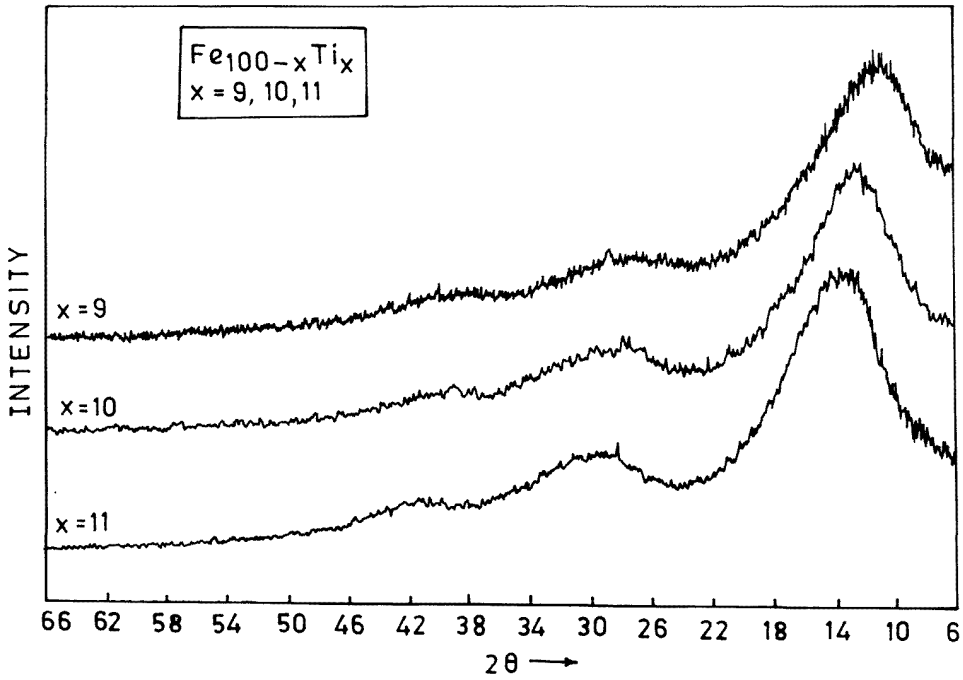

Figure 1. X-ray diffraction scans for a-$Fe_{100-x}Ti_x$ ($x = 9$, 10 and 11) alloys.

composition range from $Fe_{91}Ti_9$ to $Fe_{89}Ti_{11}$ by the DC co-sputtering method. In this paper, we report the results of detailed ferromagnetic resonance (FMR) measurements performed on a-$Fe_{100-x}Ti_x$ alloys with $x = 9$, 10 and 11. Such measurements were undertaken in order to ascertain the nature of magnetic order, low-lying magnetic excitations and anisotropy in these non-crystalline systems. Suitability of the FMR technique for the type of study intended is dictated by its capability not only to distinguish clearly [24, 26, 27] between different kinds of magnetic order (because they give rise to markedly different variations in the FMR linewidth with temperature) but also to determine unambiguously [24, 27] the type of anisotropy present.

2. Experimental details

a-$Fe_{100-x}Ti_x$ ($x = 9$, 10 and 11) films of thickness about 0.25 μm were deposited by the DC co-sputtering process onto water-cooled glass substrates under a high-purity argon pressure of 5×10^{-4} Torr. The target voltage ranged between 1 and 2 kV, and the glow discharge was sustained by a static magnetic field of magnitude 200 Oe pointing in a direction that is normal to the Ti and Fe target surfaces (facing each other) but lies within the substrate plane. The films so formed were examined by the x-ray diffraction method which makes use of Cu Kα radiation. The x-ray diffraction intensity versus angle scans taken in the range $5^\circ \leqslant 2\theta \leqslant 85^\circ$, but shown in figure 1 in the range $6^\circ \leqslant 2\theta \leqslant 66^\circ$ only because the intensity remains essentially constant at the background value for angles $66^\circ \leqslant 2\theta \leqslant 85^\circ$, reveal broad peaks characteristic of amorphous materials. The amorphous nature of the films was further confirmed by high-resolution electron microscopy (HREM) in that HREM indicated no crystalline regions.

The field derivative dP/dH of the microwave power P absorbed during the FMR process was measured as a function of the external static magnetic field H at fixed temperatures on rectangular films of typical dimensions 4 mm (length) × 3 mm (width) using horizontal–parallel ($\|^h$) and vertical–parallel ($\|^v$) sample configurations (in which H lies in the film plane and is directed along the length and width, respectively). Such measurements were carried out at a fixed microwave frequency of about 9.23 GHz on a JEOL FE3X electron spin resonance spectrometer in the temperature range 77–300 K. The sample temperature was varied between 100 and 300 K by regulating the flow of cold nitrogen gas through the annular space in the double-walled quartz jacket surrounding the quartz tube which contains the sample (the whole quartz assembly is housed within the microwave cavity). A proper gas flow was achieved by controlling the power input to a heater, immersed in a liquid-nitrogen (LN_2) container, with the aid of a proportional, integral and differential temperature controller. A pre-calibrated copper–constantan thermocouple situated outside the microwave cavity served as a control sensor while another pre-calibrated copper–constantan thermocouple in direct contact with the sample was used to monitor the sample temperature. The temperature stability achieved at the sample site was better than ±50 mK. FMR measurements at 77 K were performed by directly immersing the sample in LN_2 contained in a tailed Dewar which is in the microwave cavity. The physical quantities deduced from the dP/dH versus H curves are the resonance field H_{res}, defined as the field where the $dP/dH = 0$ line cuts the dP/dH versus H curve, and the peak-to-peak linewidth ΔH_{pp}, defined as the difference between the field values corresponding to the extrema in the dP/dH versus H curve.

H_{res} and ΔH_{pp} were measured as functions of the angle between the external static magnetic field ($\boldsymbol{H}$) direction and the sample plane or between the direction of $\boldsymbol{H}$ and the easy axis within the sample plane with the aid of a goniometer attachment (mounted on the microwave cavity) which enabled rotation and orientation of the sample plane at specific angles with respect to the direction of $\boldsymbol{H}$. Two different sample configurations, i.e. 'in-plane' (IP) and 'out-of-plane' (OP) configurations, were used. In the IP configuration, $\boldsymbol{H}$ can have any direction (specified by an angle ψ) within the sample plane with respect to the easy axis whereas, in the OP geometry, $\boldsymbol{H}$ can be oriented at any angle α in the range 0–180° with respect to the sample plane. The microwave power absorption derivative (PAD) curves were recorded at different angles in each of the two sample configurations at temperatures of 106 and 301 K. Repeated experimental runs on the sputtered films in question revealed that the reproducibility as well as accuracy with which H_{res} and ΔH_{pp} have been measured are 1% and 5%, respectively.

3. Results and discussion

Figures 2–4 depict the microwave (PAD) curves at a few representative temperatures in the range 100–300 K taken in the $\|^h$ sample configuration for a-$F_{100-x}Ti_x$ alloys with $x = 9$, 10 and 11. The PAD curves recorded in the $\|^V$ sample configuration are identical with those in these figures except for a systematic shift in the resonance field to a higher value compared with that observed in the $\|^h$ sample geometry at a given temperature. In view of the striking similarity between the sets of the data taken in the $\|^h$ and $\|^v$ sample configurations, the data taken in the former configuration alone are presented. A scrutiny of the PAD curves for different compositions in the alloys series in question (figures 2–4) reveals that such curves for the alloys with $x = 10$ and 11 consist of a *single* resonance, which shifts to higher fields and narrows as the temperature is raised from 100 to 300 K, whereas those for the alloy with $x = 9$ consist of *two resonances*, which become better resolved as the temperature is

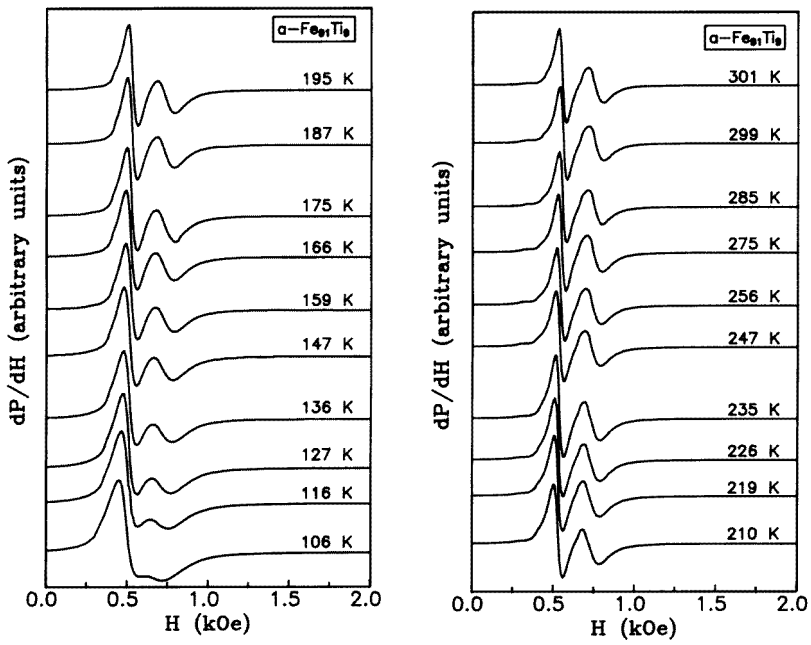

Figure 2. Microwave PAD versus applied static magnetic field curves at different temperatures in the $\|^h$ sample geometry for a-$Fe_{91}Ti_9$ alloy.

increased from 100 to 300 K. Two resonances observed in the case of the a-$Fe_{91}Ti_9$ sample at all temperatures in the range 77 K $\leqslant T \leqslant$ 300 K (note that the FMR spectrum taken at 77 K, not shown in figure 2, also exhibits a signature of the second resonance—the resonance at higher fields) obviously suggest the presence of two amorphous phases, which differ slightly in composition, in the a-$Fe_{91}Ti_9$ thin film sample. However, x-ray diffraction scans taken at room temperature (300 K) do not indicate (figure 1) the presence of two amorphous phases either in this alloy or in the other two alloy compositions ($x = 10$ and 11). From these observations, we conclude that the two amorphous phases differ appreciably only in the composition but not in the average interatomic spacings.

The realization that the observed value of resonance field H_{res} can significantly differ from the actual ('true') resonance centre when the peak-to-peak FMR linewidth ΔH_{pp} forms an appreciable fraction of H_{res}, as is at present the case (figures 2–4), necessitated a complete lineshape analysis of each resonance line separately. The Landé splitting factor g and saturation magnetization M_S were determined to an accuracy of 1% and 2%, respectively, by the lineshape analysis the details of which have been given elsewhere [24–27]. This lineshape analysis makes use of the observed values of ΔH_{pp} and those of the IP uniaxial anisotropy field H_K derived for the relation

$$H_K \simeq (H_{res}^{\|^v} - H_{res}^{\|^h})/2 \tag{1}$$

(valid for $H_K \ll 4\pi M_S$), using the measured values of resonance field in the $\|^h$ and $\|^v$ sample configurations, i.e. $H_{res}^{\|^h}$ and $H_{res}^{\|^v}$, for the alloys with $x = 10$ and 11. Since ΔH_{pp}, $H_{res}^{\|^h}$ and $H_{res}^{\|^v}$ (and hence H_K) could not be directly determined from the observed PAD curves in the case of the a-$Fe_{91}Ti_9$ thin film, all the four parameters, i.e. g, M_S, ΔH_{pp} and H_K, had to be varied in the least-squares fit computer program for the lineshape

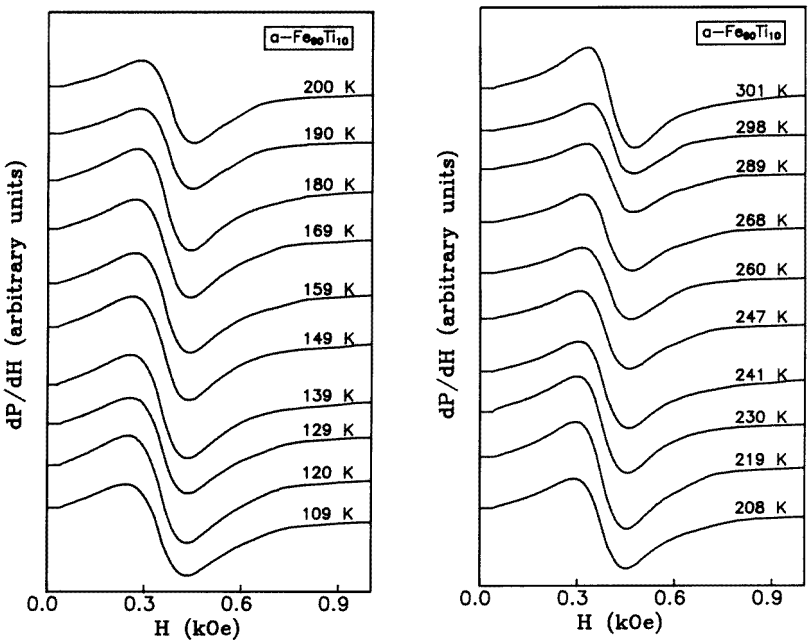

Figure 3. Microwave PAD versus applied static magnetic field curves at different temperatures in the $\|^h$ sample geometry for a-$Fe_{90}Ti_{10}$ alloy.

calculation [24–27] so as to optimize agreement with the experimental variation in $\mathrm{d}P/\mathrm{d}H$ with H. The theoretical fits so obtained are denoted by open circles in figure 5, which serves to illustrate the accuracy with which theory reproduces the experimental variation in $\mathrm{d}P/\mathrm{d}H$ with H at all temperatures for the amorphous thin films under study. Excellent agreement between theory and experiment demonstrates that the Landau–Lifshitz–Gilbert (LLG) equation of motion for magnetization (which forms the basis for theoretical lineshape calculation) adequately describes the resonant behaviour of all the compositions in the amorphous alloy series in question over the entire temperature range covered in the present investigation. Besides yielding accurate values for H_{res}, M_S and g (plus ΔH_{pp} and H_K for the alloy with $x = 9$) at different temperatures, the lineshape analysis reveals that

(i) the splitting factor g has a temperature-independent and composition-independent value of 2.07 ± 0.02,

(ii) the corrections to the observed values of H_{res} due to finite linewidth for the alloys with $x = 10$ and 11 are so small as to fall well within the uncertainty limits (about $\pm 1\%$ or less) even for temperatures as low as 77 K where ΔH_{pp} attains fairly large value,

(iii) the FMR lineshape observed at different temperatures in the range 77–300 K for a-$Fe_{91}Ti_9$ is composed of two resonances, namely the 'so-called' *primary* resonance at *lower* fields and the *secondary* resonance at *higher* fields (figure 5) and

(iv) M_S and H_K possess *higher* values in the case of the primary resonance than for the secondary resonance at all temperatures in the investigated temperature range and $H_K \simeq 0$ for the secondary resonance at temperatures ranging between 77 and 300 K.

The observation (ii) mentioned above implies that the lineshape analysis leaves the values of H_{res} (and hence of H_K) at different temperatures, obtained from the PAD curves directly for the amorphous alloys with $x = 10$ and 11, essentially *unaltered* while the

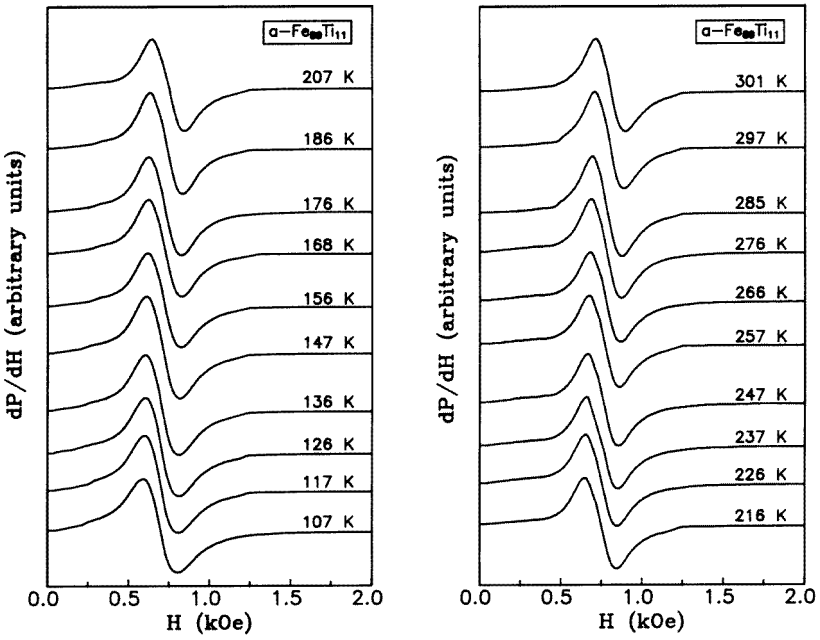

Figure 4. Microwave PAD versus applied static magnetic field curves at different temperatures in the $\|^h$ sample geometry for a-$Fe_{89}Ti_{11}$ alloy.

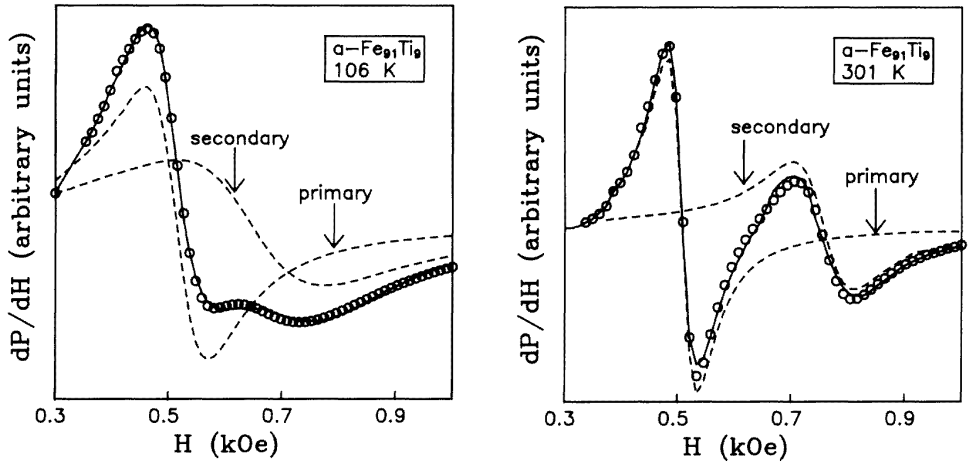

Figure 5. Microwave PAD versus applied static magnetic field curves for a-$Fe_{91}Ti_9$ taken at 106 and 301 K in the $\|^h$ sample configuration. The solid curves depict the observed variation while the open circles denote the theoretical values obtained from the lineshape calculation. Lineshape calculations reveal that the observed PAD curve at a given temperature is composed of two resonances (primary and secondary) represented by the broken curves in this figure.

lineshape calculations yield accurate values for $H_{res}(T)$, $H_K(T)$, $\Delta H_{pp}(T)$ and $M_S(T)$ (besides g) for both primary as well as secondary resonances in the case of a-$Fe_{91}Ti_9$. The functional dependences of H_{res}, ΔH_{pp}, H_K and M_S on temperature for the alloys with

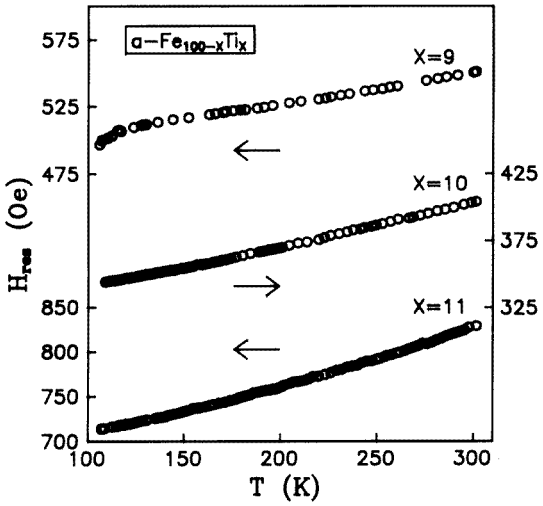

Figure 6. Temperature dependence of the resonance field H_{res} for a-$Fe_{100-x}Ti_x$ ($x = 9$, 10 and 11) films in the $\|^h$ sample geometry.

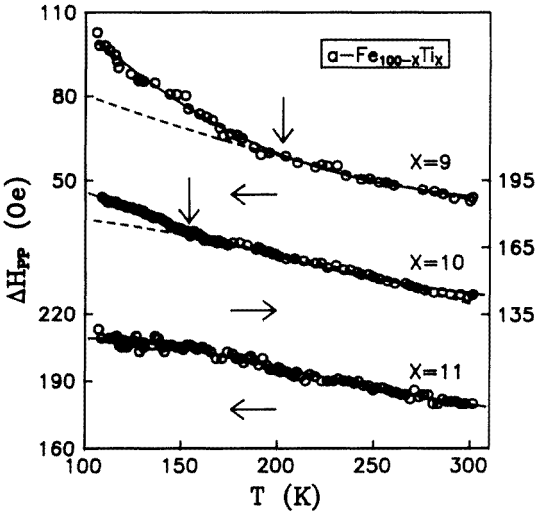

Figure 7. Variation in the 'peak-to-peak' FMR linewidth ΔH_{pp} with temperature for a-$Fe_{100-x}Ti_x$ ($x = 9$, 10 and 11) films in the $\|^h$ sample configuration. The solid curves through the data points (denoted by open circles) represent the best least-squares fits based on equation (2) of the text. The broken curves serve to highlight the onset of the upturn in $\Delta H_{pp}(T)$ at temperatures marked by downward arrows.

$x = 10$ and 11 as well as for the primary resonance for the a-$Fe_{91}Ti_9$ alloy are depicted in figures 6, 7, 8 and 9 respectively. (Figure 10 shows the corresponding data for the secondary resonance; note that $H_K \simeq 0$ for this resonance.) For reasons stated later, the data for the primary resonance in a-$Fe_{91}Ti_9$ alone are compared with the corresponding data obtained for the single resonance in the alloys with $x = 10$ and 11 in figures 6–9. Another point that deserves attention is that the Curie temperatures for the glassy alloys in question

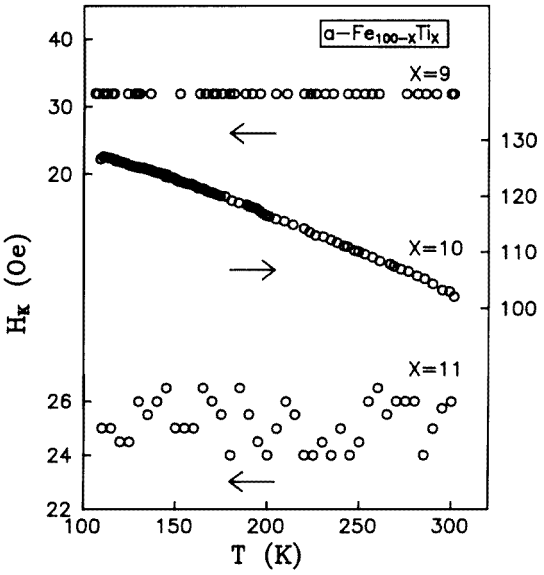

Figure 8. Variation in the IP uniaxial anisotropy field H_K with temperature for a-$Fe_{100-x}Ti_x$ ($x = 9$, 10 and 11) alloys.

lie well above 300 K, considering the present observation that the fractional reduction in $M_S(T)$ over the range 77 K $\leqslant T \leqslant$ 300 K is barely 10%.

3.1. Ferromagnetic resonance linewidth

The upturn in $\Delta H_{pp}(T)$ at low temperatures, clearly apparent for the alloys with $x = 9$ and 10 (figure 7), is reminiscent of the variation in ΔH_{pp} with temperature usually encountered in the amorphous and crystalline spin systems that exhibit re-entrant behaviour at low temperatures. In such systems, ΔH_{pp} is found [35–37] to vary with temperature in accordance with the expression [35–38]

$$\Delta H_{pp}(x, \nu, T) = \Gamma_0(x, \nu) + \Gamma_1(x, \nu)[T/T_0(x, \nu)] \exp[-T/T_0(x, \nu)] \qquad (2)$$

which is based on the infinite ferromagnetic matrix plus finite ferromagnetic clusters model [4, 16, 39–41]. In equation (2), Γ_0 is the value of linewidth in the intermediate-temperature range where it is either temperature independent or weakly dependent on temperature, Γ_1 is a parameter which, among other physical quantities, depends on the number of spins per unit volume in the infinite ferromagnetic cluster and the anisotropic interactions between the spins of the finite clusters and those of the infinite cluster, and T_0 is the temperature at which the finite clusters freeze in random orientations; Γ_0, Γ_1 and T_0 all depend on the concentration x of the magnetic atoms in the alloy system and the microwave-field frequency ν. The continuous curves through the $\Delta H_{pp}(T)$ data points shown in figures 7 and 10 represent the best least-squares fits based on equation (2) with the choice of parameters Γ_0, Γ_1 and T_0 given in table 1. The very fact that the observed variation on ΔH_{pp} with temperature is closely reproduced by the theoretical variation predicted by equation (2) strongly suggests that the amorphous alloys in question exhibit re-entrant behaviour at low temperatures. Moreover, the theoretical variations (figures 7 and 10), when extrapolated to 77 K, yield values which conform well with the observed data at that temperature for all the three

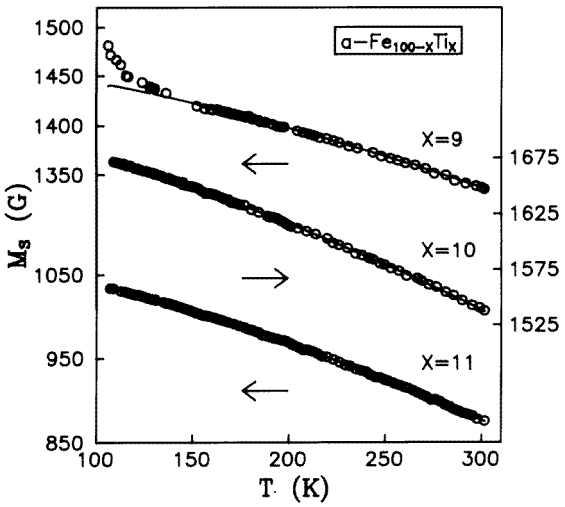

Figure 9. Variation in M_S with temperatures for a-$Fe_{100-x}Ti_x$ ($x = 9$, 10 and 11) alloys. The solid curves through data points (denoted by open circles) are the best least-squares fits to the data taken in the temperature range 100 K $\leqslant T \leqslant$ 300 K (50 K $\leqslant T \leqslant$ 300 K for the alloy with $x = 9$) based on equation (4) of the text with $D(T) = D(0)$ and $\beta = 0$.

compositions. An increase (decrease) in the value of Γ_1 (T_0) as the concentration of Fe is increased (table 1) has also been previously observed [24, 27] in a-$Fe_{100-x}Zr_x$ alloys in the same concentration range as the present one. At this stage, it should be pointed out that equation (2) is strictly valid only for $T \ll T_0$ but this expression fits the $\Delta H_{pp}(T)$ data even for $T \gg T_0$. Extensive study [24, 26, 27] of the homologous alloy system, i.e. a-$Fe_{100-x}Zr_x$, has revealed that, contrary to the theoretical predictions [38], a direct relation between T_0 and the re-entrant transition temperature T_{RE} does not exist. Generally, in re-entrant systems, the upturn in $\Delta H_{pp}(T)$ starts at a temperature of about $2T_{RE}$ so that the data presented in figures 7 and 10 indicate that T_{RE} shifts to lower temperature as x increases.

3.2. 'In-plane' uniaxial anisotropy field

At first sight, the temperature dependences of H_K and M_S shown in figures 8 and 9 might seem to suggest that H_K bears no relationship with M_S but, when $H_K(T)$ is plotted

Table 1. Parameter values for the fits to the $\Delta H_{pp}(T)$ data based on equation (2) of the text. The numbers in parentheses denote the error in the least significant figure. The abbreviations P and S stand for the primary and secondary resonances, respectively.

Composition	Γ_0 (Oe)	Γ_1 (Oe)	T_0 (K)
$Fe_{89}Ti_{11}$	159.9 (21)	134.4 (26)	98.8 (12)
$Fe_{90}Ti_{10}$	135.7 (23)	153.0 (25)	70.0 (10)
$Fe_{91}Ti_9$(P)	139.4 (26)	214.2 (28)	54.9 (11)
$Fe_{91}Ti_9$(S)	143.0 (25)	153.0 (25)	59.4 (16)

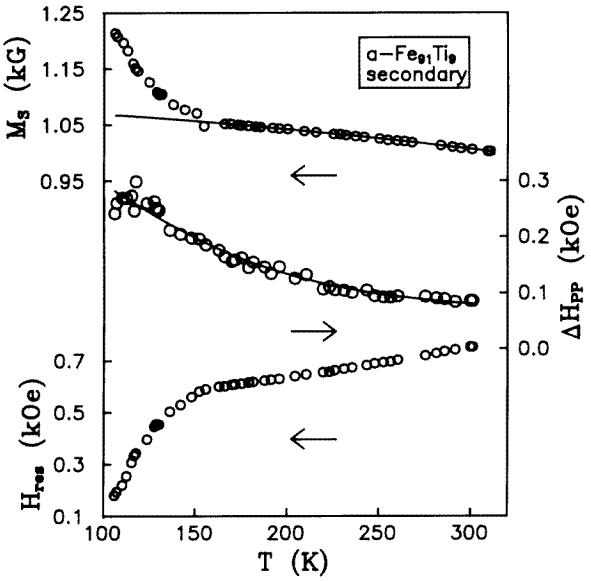

Figure 10. Variations in resonance field H_{res}, linewidth ΔH_{pp} and M_S with temperature for the secondary resonance in a-$Fe_{91}Ti_9$ alloy. The open circles denote the data points while the solid curves depict the theoretical variations predicted by equations (2) and (4) with $\beta = 0$, $D(T) = D(0)$ and the choice of parameters given in tables 1 and 2.

against $M_S(T)$ in figure 11 for a-$Fe_{90}Ti_{10}$, a linear relation between them becomes apparent. However, the same type of proportionality between $H_K(T)$ and $M_S(T)$ is not evident for the remaining two compositions unless cognizance is taken of the following remarks. In the present measurements, the field H in the $\mathrm{d}P/\mathrm{d}H$ versus H scans cannot be resolved to better than 2.5 Oe. Thus, the smaller the value of H_K, the greater is the error in the determination of H_K. To elucidate this point further, for the alloys with $x = 9$ and 11, H_K has temperature-independent values of 32 ± 2.5 Oe (for the primary resonance) and 25 ± 2.5 Oe, respectively, so that the change in H_K with temperature, if any, can be detected only when the percentage change exceeds 16% and 20% for the compositions $x = 9$ and 11. Now that the percentage change in M_S between 100 and 300 K, i.e. $100\{[M_S(100\ \mathrm{K}) - M_S(300\ \mathrm{K})]/M_S(100\ \mathrm{K})\}$, is 7% (for the primary resonance) and 16% for the alloys with $x = 9$ and 11, a similar change in the quantity H_K, i.e. $100\{[H_K(100\ \mathrm{K}) - H_K(300\ \mathrm{K})]/H_K(100\ \mathrm{K})\}$, will go undetected because it falls well within the uncertainty limits set by the resolution of H. Thus, the observed temperature variations in H_K and M_S in these two alloys do not exclude the possibility that $H_K(T) \propto M_S(T)$. In this context, it is important to note that, at any given temperature in the range 100–300 K, H_K, like M_S, goes through a peak at $x = 10$ as a function of Ti concentration x. A linear relation of the type

$$H_K(T) = \alpha M_S(T) \tag{3}$$

which is found to hold for a large number of amorphous ferromagnets [42–47], is a characteristic property of long-range ferromagnetic order. Equation (3) permits calculation of the uniaxial anisotropy constant $K_u(T)$, when the value of the constant α, i.e. the slope of the least-squares fit straight line through the data in a $H_K(T)$ versus $M_S(T)$ plot (figure 11), is used in equation (3) and $H_K(T)$ is set equal to $2K_u(T)/M_S(T)$. The value of K_u at 77 K computed in this way for the alloy with $x = 10$ turns out to be 2.60×10^5 erg cm^{-3}.

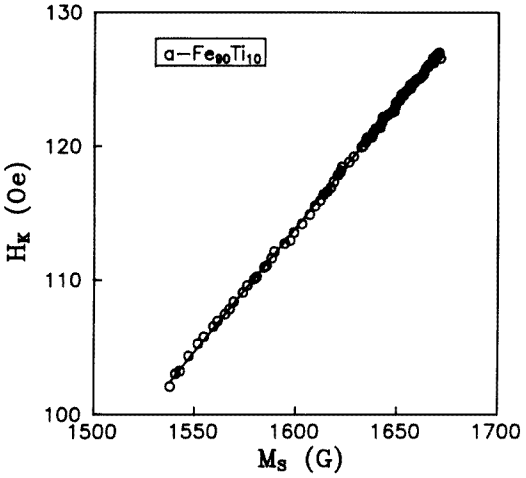

Figure 11. $H_K(T)$ as a function of $M_S(T)$. The straight line through the data points represents the best least-squares fit to the data based on equation (3) of the text.

Similar values have been reported [42–47] for K_u in many amorphous systems. However, for melt-spun a-$Fe_{90}Zr_{10}$, $K_u(77\ \mathrm{K}) = (2.91 \pm 0.40) \times 10^4$ erg cm^{-3} [24]. The validity of equation (3) in the present case indicates that the coupling energy of the anisotropy is dipolar in origin, i.e. this anisotropy probably results from the atomic pair ordering [42, 47] which may have been introduced during the rapid solidification process in the presence of an applied field of magnitude 200 Oe. Considering that M_S has a value as high as 1000 G (figure 10) while $H_K \simeq 0$ in the entire temperature range 77 K $\leqslant T \leqslant$ 300 K for the secondary resonance in the alloy with $x = 9$, the relation between H_K and M_S of the form equation (3) breaks down completely. The observation that $H_K = 0$ implies that the magnetization vector of the amorphous ferromagnetic phase that gives rise to the secondary resonance has no preferred direction in the sample plane in the absence of an external magnetic field. Moreover, widely different values of M_S and H_K for the two magnetic phases in a-$Fe_{91}Ti_9$ are manifestations of the distinctly different chemical and geometrical short-range order in the two amorphous phases. In this respect, the secondary resonance differs from not only the primary resonance in a-$Fe_{91}Ti_9$ thin film but also the single resonance observed in the other compositions in the present alloy series. In order that a comparison between different sets of data is meaningful, the $H_{res}(T)$, $\Delta H_{pp}(T)$, $H_K(T)$ and $M_S(T)$ data for the primary resonance alone are included in figures 6–9 together with similar data on the remaining compositions whereas the variations in H_{res}, ΔH_{pp} and M_S with temperature for the secondary resonance are separately shown in figure 10.

3.3. Saturation magnetization and low-lying magnetic excitations

With a view to identifying the types of 'low-lying' magnetic excitations that are primarily responsible for the decline of magnetization with increasing temperature and to determine the relative magnitudes of their contributions to thermal demagnetization in different temperature ranges, an elaborate data analysis, the details of which have been given elsewhere [4, 14, 27, 48], of the $M_S(T)$ data, shown in figures 9 and 10. was carried out.

As a part of this exercise, the expression

$$\frac{M(H,0)-M(H,T)}{M(H,0)} = \frac{g\mu_B}{M(H,0)}\left[Z(\tfrac{3}{2},t_H)\left(\frac{k_BT}{4\pi D(T)}\right)^{3/2} + 15\pi\beta Z(\tfrac{5}{2},t_H)\left(\frac{k_BT}{4\pi D(T)}\right)^{5/2}\right] \tag{4}$$

has been least-squares fitted to the $M_S(T)$ data in the temperature ranges 150 K $\leqslant T \leqslant$ 300 K, 100 K $\leqslant T \leqslant$ 300 K and 77 K$\leqslant T \leqslant$300 K for the alloys with $x = 9$, 10 and 11, respectively. In equation (4), the Bose–Einstein integral function

$$Z(s,t_H) = \sum_{n=1}^{\infty} n^{-s}\exp(-nt_H) \tag{5}$$

with $t_H = T_g/T = g\mu_B H_{eff}/k_BT$, accounts for the extra energy gap $k_BT_g = g\mu_B H_{eff}$ in the spin-wave (SW) spectrum arising from the effective field $H_{eff} = H - 4\pi NM + H_K$ (where N, M and H_K are the demagnetizing factor, magnetization and anisotropy field, respectively) which the spins experience within the sample. The main outcome of such least-squares fits is that the $T^{3/2}$ term in equation (4) without the temperature renormalization of the SW stiffness coefficient D, i.e. by setting $D(T) = D(0)$ (the value of D at 0 K), alone provides the best least-squares fit to the $M_S(T)$ data in the above-mentioned temperature ranges with the choice of parameters $M_S(0)$ and $D(0)$ given in table 2. $M_S(0)$ and $D(0)$ are plotted against Fe concentration in figure 12. It is noticed from this figure that $M_S(0)$ goes through a peak (at $x = 10$) as a function of x while $D(0)$ *increases* with decreasing x. By comparison, $M_S(x)$ has essentially the same functional form but $D(0)$ decreases with decreasing x in a-$Fe_{100-x}Zr_x$ alloys with x in the range $8 \leqslant x \leqslant 12$ [4, 14, 19]. A pictorial demonstration of this result is provided by the M_S versus $T^{3/2}$ plots displayed in figure 13 which are evidently *linear* in the temperature ranges mentioned above. The solid straight lines drawn through the data points in this figure and the solid curves in figures 9 and 10 represent the best theoretical least-squares fits to the data based on equation (4) with the choice of parameters given in table 2. Close agreement between theory and experiment in the specified temperature ranges obviously implies that SW excitations alone completely account for the observed thermal demagnetization. In arriving at these fits, the values of g and the anisotropy field H_K determined at present as well as knowledge of the demagnetization factors from low-field ($H \leqslant 10$ Oe) magnetization data have been used to calculate the effective field H_{eff} and the value of H_{eff} so obtained is, in turn, used to compute the Bose–Einstein integral function $Z(3/2, t_H)$. In figures 9, 10 and 13, the data point taken at 77 K for each composition is deliberately omitted so that the data in the temperature range 100 K $\leqslant T \leqslant$ 300 K could be plotted on a more sensitive scale. If the theoretical variation in M_S with T is extrapolated to 77 K, the data point at 77 K falls on the theoretical curve only for the alloy with $x = 11$ but not for the remaining two compositions for which it lies above. A sudden increase in $M_S(T)$ as the temperature is lowered below 150 K in a-$Fe_{91}Ti_9$ (figures 9 and 10) signals a progressive decrease in the value of SW stiffness and hence *softening* of the *SW modes*, as the temperature is decreased through $T_{RE} \simeq$ 150 K. The same explanation could be offered for the observation that the value of M_S at 77 K for the alloy with $x = 10$ exceeds that expected on the basis of the Bloch $T^{3/2}$ variation with the value of SW stiffness obtained in the temperature range 100 K $\leqslant T \leqslant$ 300 K. In view of this argument, it seems that T_{RE} for a-$Fe_{90}Ti_{10}$ lies between 77 and 100 K whereas for a-$Fe_{89}Ti_{11}$ it lies below 77 K. This inference is in conformity with the general observation [16, 24, 27] that the onset of the sudden increase in $\Delta H_{pp}(T)$ at low

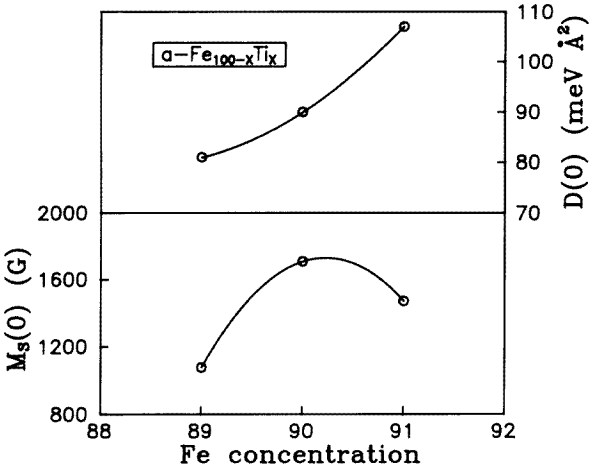

Figure 12. Variations in saturation magnetization $M_S(0)$ and SW stiffness coefficient $D(0)$ at 0 K with Fe concentration in a-$Fe_{100-x}Ti_x$ ($x = 9$, 10 and 11) alloys.

Table 2. SW parameters for the alloys investigated. The numbers in parentheses denote the error in the least significant figure. P and S stand for the primary and secondary resonances, respectively.

Composition	$M_S(0)$ (G)	$D(0)$ (meV Å^2)
$Fe_{89}Ti_{11}$	1077 (2)	81 (2)
$Fe_{90}Ti_{10}$	1709 (2)	91 (2)
$Fe_{91}Ti_9$(P)	1469 (2)	107 (3)
$Fe_{91}Ti_9$(S)	1108 (2)	134 (3)

temperatures lies consistently *higher* than the value of T_{RE} determined from the temperature dependence of M_S. Within the framework of the model proposed by Kaul [4, 16, 39–41], this finding indicates that the freezing of finite spin clusters in random orientations starts at a temperature well above T_{RE} and the freezing process takes place over a wide temperature range rather than abruptly at a certain well defined temperature. Hence, the transition to the re-entrant state (which is a mixed state in which cluster spin glass order coexists with long-range ferromagnetic order) is not a true thermodynamic phase transition in that the finite spin clusters do not cooperatively freeze in random orientations abruptly at temperature T_{RE} but instead the freezing process is a thermally activated process which occurs over a wide temperature range. This implies that, as the temperature is lowered below room temperature (in the present case), the largest cluster freezes first and subsequently smaller and smaller clusters freeze in random directions as their relaxation rate slows down so much so that they do not have sufficient thermal energy to overcome the potential barrier brought into existence by the frozen larger clusters. The same inference has recently been drawn for the FMR [24, 27] and Mössbauer [14, 16] data on a-$Fe_{100-x}Zr_x$ ($9 \leqslant x \leqslant 11$) alloys. Moreover, T_{RE} decreases with increasing x in Fe-rich a-$Fe_{100-x}Zr_x$ alloys, as it does in the present case.

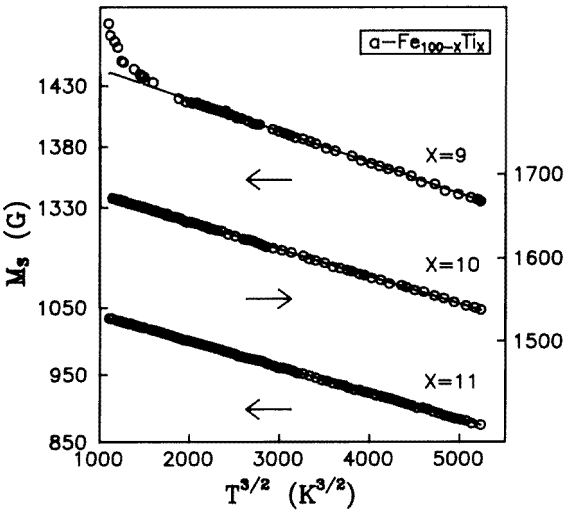

Figure 13. SW $T^{3/2}$ (Bloch power law) dependence of saturation magnetization for a-$Fe_{100-x}Ti_x$ ($x = 9$, 10 and 11) films. The solid curves through the data points represent the least-squares fits to the data, based on equation (4) of the text with $D(T) = D(0)$ and $\beta = 0$, in the temperature range 150 K $\leqslant T \leqslant$ 300 K for the alloy with $x = 9$ and 100 K $\leqslant T \leqslant$ 300 K for the remaining two compositions.

3.4. Angular dependence of the resonance field and linewidth

As already mentioned in section 2, the PAD curves for each composition in the investigated alloy series have been recorded as a function of either the angle ψ between the external static magnetic field H direction and the easy axis within the sample plane (i.e. the IP case) or the angle α between the direction of H and the sample plane (i.e. the OP case) at two fixed values of temperature, i.e. $T = 106$ K and $T = 300$ K. Since the angular dependences of the PAD curves (and hence of the derived quantities H_{res} and ΔH_{pp}) are almost the same for both these temperatures, only the $\mathrm{d}P/\mathrm{d}H$ versus H curves recorded at $T = 300$ K for a few representative values of the angles ψ and α are presented and discussed in this section. Such curves obtained in the IP case for a-$Fe_{91}Ti_9$ and a-$Fe_{89}Ti_{11}$ are shown in figures 14 and 15. A similar figure for the a-$Fe_{90}Ti_{10}$ film is not presented because the angular dependence of lineshapes observed for this alloy is similar to that for a-$Fe_{89}Ti_{11}$. A cursory glance at figure 14 suffices to reveal that both H_{res} and ΔH_{pp} for the secondary resonance in a-$Fe_{91}Ti_9$ are nearly *independent* of the angle ψ. An immediate consequence of this result is that $H_K \simeq 0$ for this resonance. This observation is consistent with our earlier finding that $H_{res}^{\parallel^h}(T) \simeq H_{res}^{\parallel^v}(T)$ for the secondary resonance (section 3.1). The angular dependences of H_{res} and ΔH_{pp} at $T = 300$ K in the IP case for the alloys with $x = 9$ and $x = 11$ are depicted in figures 16 and 17, respectively. While H_{res} as a function of angle ψ (for definition of angle ψ see figure 18) goes through a peak at $\psi = 90^\circ$, $\Delta H_{pp}(\psi)$ exhibits a minimum at the same value of ψ. The curves drawn through the data points in figure 16 represents the best theoretical least-squares fits to the data that are arrived at by the following procedure. First, the equilibrium condition [28]

$$\frac{\sin\psi}{\sin\phi} - \frac{\cos\psi}{\cos\phi} - \frac{H_K}{H_{res}} = 0 \tag{6}$$

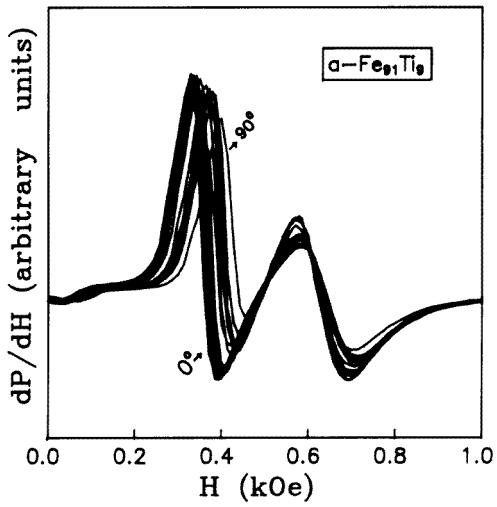

Figure 14. dP/dH versus H curves at various angles ψ in the IP geometry for the a-$Fe_{91}Ti_9$ alloy film.

is solved for a given value of the angle ψ, the observed value of H_{res} at that ψ and a trial value of H_K to yield the corresponding value of the angle ϕ (figure 18). The value of ϕ so obtained is inserted into the resonance condition [28]

$$(\omega/\gamma)^2 = [H_{res}\cos(\psi-\phi) + 4\pi M_S + H_K\cos^2\phi][H_{res}\cos(\psi-\phi) + H_K\cos(2\phi)] \quad (7)$$

(where $\gamma = g\mu_B/\hbar$ is the gyromagnetic ratio, μ_B is the Bohr magneton and $\omega = 2\pi\nu$ is the microwave field frequency) and M_S and H_K are then varied in the least-squares fit computer program so as to optimize agreement with the value H_{res} observed at that particular value of the angle ψ. The value of H_K obtained in this way is inserted back into equation (6) to compute the angle ϕ whose value is again used in equation (7) to deduce the refined values of M_S and H_K. This iteration procedure is continued until agreement with the experimental values of H_{res} at a given value of the angle ψ is optimized. In other words, equations (6) and (7) are self-consistently solved in order to arrive at the optimal values of M_S and H_K (listed in table 3) that corresponds to the theoretical fits shown in figure 16. The dP/dH versus H curves at a few representative values of the angle α (for definition of this angle, see figure 18) in the OP case for a-$Fe_{100-x}Ti_x$ ($x = 9$, 10 and 11) are shown in figures 19–21. The variations in H_{res} and ΔH_{pp} with the angle α for the samples in question, deduced from the observed PAD curves (figures 19–21), are displayed in figures 22 and 23, respectively. It is obvious from the data presented in figures 16 and 22 that, while the variation in H_{res} in the IP case as the angle ψ is swept from 0° to 180° is less than 100 Oe, H_{res} changes by more than an order of magnitude from its value at $\alpha = 0°$ or 180° when α is increased from 0° to 180° through $\alpha = 90°$ in the OP case. A similar variation with the angles ψ and α is also observed for ΔH_{pp} (figures 17 and 23). The break in the $H_{res}(\alpha)$ and $\Delta H_{pp}(\alpha)$ curves in figures 22 and 23 for the angles in the vicinity of 90° should not be interpreted as a signature of divergence since H_{res} and ΔH_{pp} for the angles in this range exceed the highest magnetic field (11 kOe) generated by the electromagnet coupled to the spectrometer. The theoretical fits, denoted by the solid curves in figure 22, as in the IP case, are obtained by self-consistently solving the expressions [28]

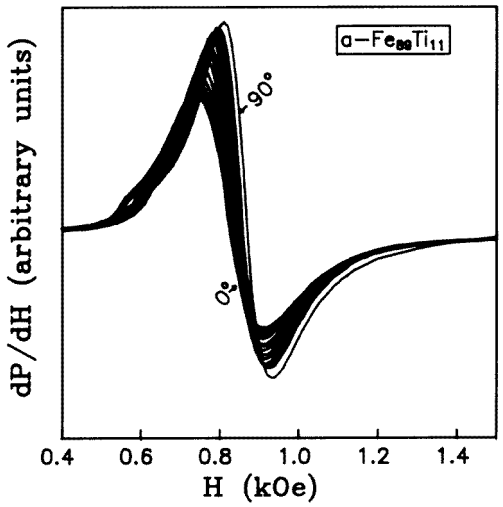

Figure 15. $\mathrm{d}P/\mathrm{d}H$ versus H curves at various angles ψ in the IP geometry for the a-$Fe_{91}Ti_{11}$ alloy film.

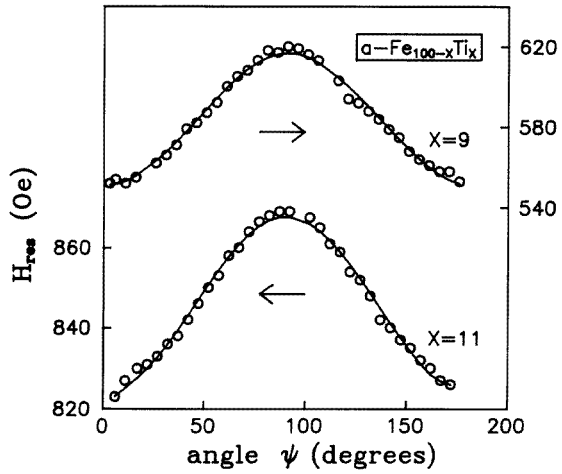

Figure 16. Variation in the resonance field H_{res} with angle ψ in the IP geometry. The solid curves through the data points (denoted by open circles) are the best least-squares fits based on equations (6) and (7) of the text.

$$\frac{\sin\alpha}{\sin\theta} - \frac{\cos\alpha}{\cos\theta} - \frac{4\pi M_S + H_K}{H_{res}} = 0 \tag{8}$$

and

$$(\omega/\gamma)^2 = [H_{res}\cos(\alpha-\theta) + (4\pi M_S + H_K)\cos(2\theta)] \times [H_{res}\cos(\alpha-\theta) - 4\pi M_S \sin^2\theta + H_K\cos^2\theta] \tag{9}$$

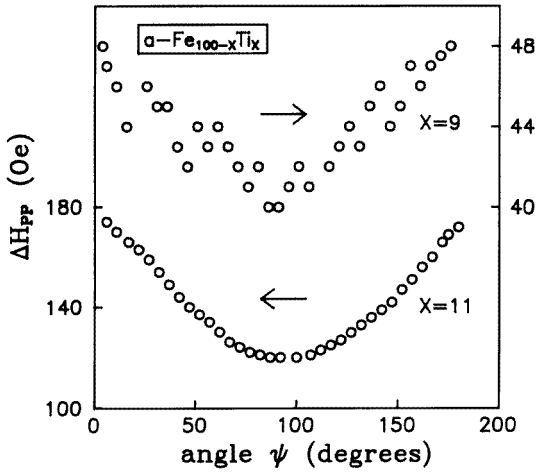

Figure 17. Variation in ΔH_{pp} with angle ψ in the IP geometry.

Table 3. Comparison of M_S and H_K values deduced from the lineshape analysis of the FMR spectra with those determined from the IP and OP angular dependences of the resonance field at $T = 300$ K. The numbers in parentheses and the symbols P and S have the same meaning as in tables 1 and 2.

	M_S (G)			H_K (Oe)		
Composition	Lineshape analysis	IP case equations (6) and (7)	OP case equations (8) and (9)	Lineshape analysis equation (1)	IP case equations (6) and (7)	OP case equations (8) and (9)
$Fe_{89}Ti_{11}$	876 (8)	886 (14)	902 (27)	25 (5)	22 (3)	20 (5)
$Fe_{90}Ti_{10}$	1537 (23)	1565 (15)	1593 (32)	92 (5)	95 (4)	101 (7)
$Fe_{91}Ti_9$(P)	1336 (10)	1335 (10)	1330 (20)	32 (5)	33 (3)	40 (6)
$Fe_{91}Ti_9$(S)	1012 (23)	1020 (13)	1050 (26)	0 (1)	0 (1)	1 (1)

for M_S and H_K. The values of M_S and H_K arrived at in this way are listed in table 3 while the equilibrium values of θ (the angle between the equilibrium direction of magnetization and the sample plane) at different values of α (the angle between the external static magnetic field and the sample plane in the OP case) are plotted in the form of θ versus α curves in figure 24 for the a-$Fe_{100-x}Ti_x$ alloys with $x = 9$, 10 and 11. It is noticed from this figure that, for $\alpha \lesssim 70^\circ$, the direction of the magnetization vector is not significantly altered (i.e. the magnetization vector lies very close to the sample plane) but, as α increases beyond 70°, the magnetization vector abruptly changes its direction so as to follow the variations in the field direction. This finding is a manifestation of the fact that the external field is able to overcome the anisotropy (shape and uniaxial anisotropies) forces only when α exceeds 70°. Table 3 compares the values of M_S and H_K deduced from the angular dependence of H_{res} in the IP and OP cases with those extracted from the lineshape analysis of the FMR spectra taken at $T = 300$ K (in the case of H_K, such a comparison is also made with the values of H_K obtained from equation (1)). That the different sets of data are in striking agreement with one another emphasizes the fact that the quantities M_S and H_K, like other physical parameters H_{res} and ΔH_{pp}, have been determined accurately in this work.

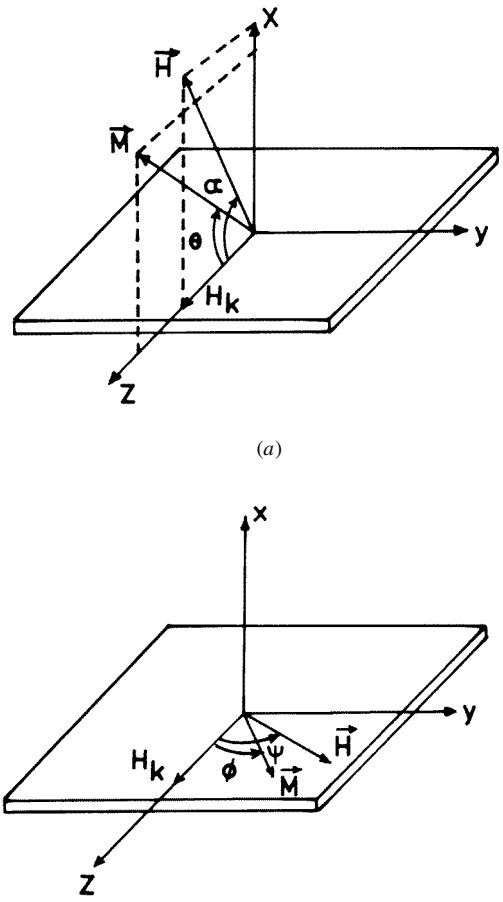

Figure 18. Coordinate system showing various angles used in the computation of angular variation of resonance field for the (*a*) OP and (*b*) IP cases.

Calculations leading to the theoretical expressions for $\Delta H_{pp}(\psi)$ and $\Delta H_{pp}(\alpha)$ are not as straightforward as those outlined above for $H_{res}(\psi)$ and $H_{res}(\alpha)$ for the following reasons. First, as the frequency of the microwave field is held constant and the applied static magnetic field H is swept through resonance in the present experiments, corrections have to be made for the fact that $\boldsymbol{M}$ and $\boldsymbol{H}$ are not collinear, so that the change in the applied field is not the same as the change in the *effective* field. Second, as H changes, the direction of $\boldsymbol{M}$ changes, giving rise to an apparent line broadening which must be taken into account as well. Such corrections are small in the IP case because the angles in question are small. However, this is not the case in the OP geometry because $\boldsymbol{M}$ goes out of the sample plane, the demagnetizing fields are large and corrections to the 'raw' linewidth data are appreciable. The main complication, particularly in the case of amorphous ferromagnets, arises from the fact that an unambiguous separation of frequency-independent and frequency-dependent (LLG) components of FMR linewidth is not possible unless FMR measurements are carried out at different microwave-field frequencies. Since the present

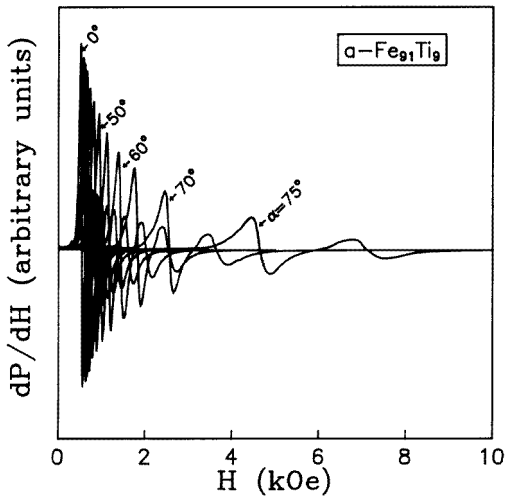

Figure 19. dP/dH versus H curves at various angles α in the OP geometry at 300 K for the a-$Fe_{91}Ti_9$ alloy film.

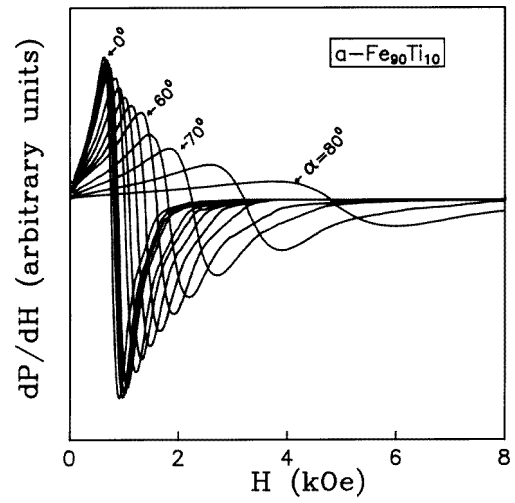

Figure 20. dP/dH versus H curves at various angles α in the OP geometry at 300 K for the a-$Fe_{90}Ti_{10}$ alloy film.

measurements were performed at a single fixed value of the microwave-field frequency, the relative magnitudes of the two contributions to ΔH_{pp} could not be determined. To make matters worse, the above corrections affect the angular dependences of these contributions differently. Thus, theoretical fits to the $\Delta H_{pp}(\psi)$ and $\Delta H_{pp}(\alpha)$ data displayed in figures 17 and 23, respectively, could not be attempted.

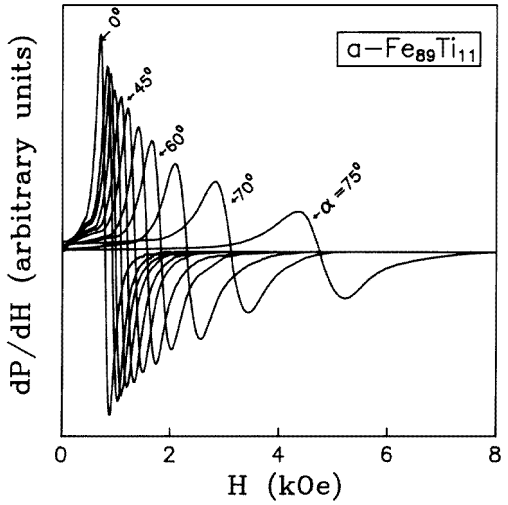

Figure 21. dP/dH versus H curves at various angles α in the OP geometry at 300 K for the a-$Fe_{89}Ti_{11}$ alloy film.

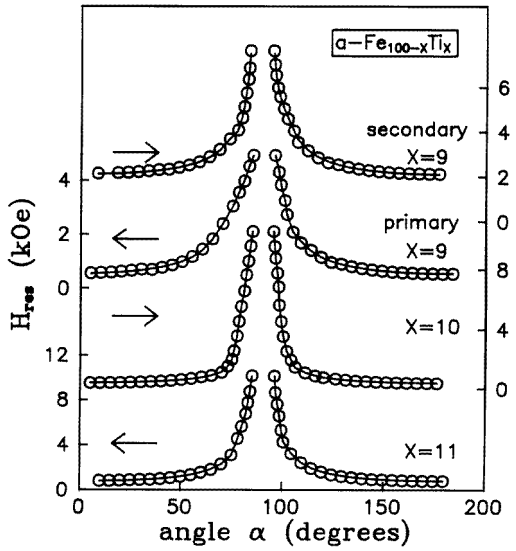

Figure 22. Variation in resonance field H_{res} with angle α in the OP geometry. The solid curves represent the fits based on equations (8) and (9) of the text.

4. Conclusion

Detailed FMR measurements have been performed on a-$Fe_{100-x}Ti_x$ alloys with $x = 9$, 10 and 11 in the $\|^h$ and $\|^v$ sample configurations at a fixed microwave-field frequency of almost 9.23 GHz in the temperature range 77–300 K. The main results obtained and conclusions drawn from them are summarized below.

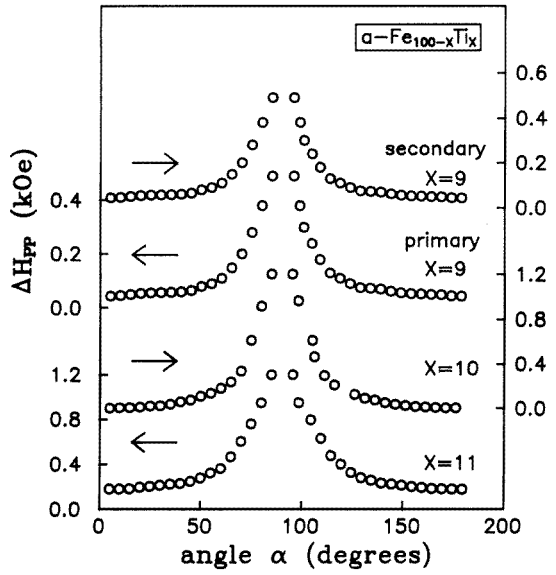

Figure 23. Variation in 'peak-to-peak' linewidth ΔH_{pp} with angle α in the OP geometry.

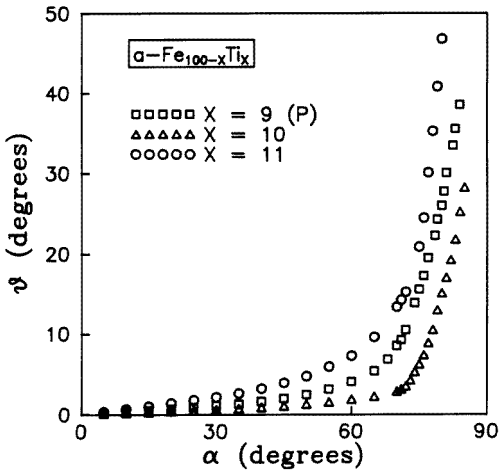

Figure 24. Variation in magnetization angle θ with α, the angle between the external static magnetic field direction and the sample plane, in the OP geometry.

(I) While a single resonance is observed in the entire temperature range of present investigation for the alloys with $x = 10$ and 11, FMR spectra taken at temperatures in the range 77–300 K on a-$Fe_{91}Ti_9$ consist of two resonances (primary and secondary resonances) which have different properties. The IP uniaxial anisotropy field H_K scales with the saturation magnetization M_S in the temperature range 77 K $\leqslant T \leqslant$ 300 K for the primary resonance in a-$Fe_{91}Ti_9$ and for the resonance observed in the amorphous thin films with $x = 10$ and 11. This result is taken to imply that the anisotropy energy is of dipolar origin. The relation $H_K \propto M_S$, however, breaks down in the case of secondary resonance

because $H_K \simeq 0$ while M_S is of sizeable magnitude for this resonance. Throughout the temperature range 77 K $\leqslant T \leqslant$ 300 K, M_S for the secondary resonance is consistently lower than the primary resonance. It is argued that the primary and secondary resonances originate from two distinctly different amorphous magnetic phases which widely differ in their chemical as well as geometrical short-range orders.

(II) Detailed lineshape analysis of each FMR spectrum separately yields accurate values for the Laudé splitting factor g, M_S, H_{res} and H_K at different temperatures for all the alloys investigated. The splitting factor has a temperature-independent and composition-independent value of $g = 2.07 \pm 0.02$.

(III) SW excitations give a dominant contribution to the thermal demagnetization in the temperature range $T_{RE} \leqslant T \leqslant 300$ K. As the temperature is lowered below T_{RE}, the saturation magnetization increases at a rate faster than that suggested by the SW (Bloch) $T^{3/2}$ variation observed for $T > T_{RE}$. The temperature T_{RE}, below which an upturn in $M_S(T)$ is observed, marks the onset of the re-entrant behaviour. An upturn in $M_S(T)$ for $T < T_{RE}$ is an indication of the softening of the SW modes. Consistent with this inference, the 'peak-to-peak' linewidth ΔH_{pp} also exhibits a temperature dependence that is characteristic of re-entrant spin systems. T_{RE} decreases with increasing x, indicating thereby that the re-entrant behaviour is progressively suppressed as the Ti concentration is increased. These observations find a straightforward explanation in terms of the infinite ferromagnetic matrix plus finite ferromagnetic spin clusters model which demonstrates that the freezing process is a thermally activated process and that the transition to the re-entrant state is not a true thermodynamic phase transition.

(IV) IP and OP angular dependences of the resonance field as well as the FMR spectra taken at a given temperature in the $\|^h$ and $\|^v$ sample configurations all yield the same (within the uncertainty limits) values of M_S and H_K.

References

[1] Kaul S N 1983 *Phys. Rev.* B **27** 6923
[2] Fukamichi K 1983 *Amorphous Metallic Alloys* ed F E Luborsky (London: Butterworth) p 317
[3] Fukamichi K, Hiroyoshi H, Shirakawa K, Masumoto T and Kaneko T 1986 *IEEE Trans. Magn.* **22** 424
[4] Kaul S N 1991 *J. Phys.: Condens. Matter* **3** 4027
[5] Kaul S N, Babu P D, Seeger M and Kronmüller H 1997 *Phys. Rev.* B at press
[6] Shirakawa K, Ohnuma S, Nose M and Masumoto T 1980 *IEEE Trans. Magn.* **16** 910
[7] Fukamichi K, Kikuchi M and Masumoto T 1984 *J. Non-Cryst. Solids* **61–2** 961
[8] Fukamichi F and Hiroyoshi H 1985 *Sci. Rep. Res. Inst. Tokoku Univ.* A **33** 154
[9] Hiroyoshi H and Fukamichi 1982 *J. Appl. Phys.* **53** 2226
[10] Deppe P, Fukamichi K, Li F S, Rosenberg M and Sostarich M 1984 *IEEE Trans, Magn.* **20** 1367
[11] Hiroyoshi H, Noguchi K, Fukamichi K and Nakagawa Y 1985 *J. Phys. Soc. Japan* **54** 3554
[12] Ryan D H, Coey J M D and Ström-Olsen J O 1987 *J. Magn. Magn. Mater.* **67** 148
Ryan D H, Ström-Olsen J O, Muir W B, Cadogan J M and Coey J M D 1989 *Phys. Rev.* B **40** 11 208
[13] Ghafari M, Keune W, Brand R A, Day R K and Dunlop J B 1988 *Mater. Sci. Eng.* **99** 65
Ghafari M, Chmielek N, Keune W and Foley C P 1989 *Physica* B **161** 222
[14] Kaul S N, Siruguri V and Chandra G 1992 *Phys. Rev.* B **45** 12 343
[15] Kiss L F, Kemény T, Vincze I and Gránásy L 1994 *J. Magn. Magn. Mater.* **135** 161
[16] Kaul S N 1995 *Met. Mater. Proc.* **7** 29
[17] Yamamoto H, Onodera H, Hosoyama K, Masumoto T and Yamauchi H 1983 *J. Magn. Magn. Mater.* **31–4** 1579
[18] Day R K, Dunlop J B, Foley C P, Ghafari M and Pask H 1985 *Solid State Commun.* **56** 843
[19] Ryan D H, Coey J M D, Batalla E, Altounian Z and Stöm-Olsen J O 1987 *Phys. Rev.* B **35** 8630
[20] Kaul S N, Bansal C, Kumaran T and Havakgi M 1988 *Phys. Rev.* B **38** 9248
[21] Read D A, Moyo T, Jassim S, Dunlop R A and Hallam G C 1989 *J. Magn. Magn. Mater.* **82** 87
[22] Siruguri V, Kaul S N, Rajaram G and Chandra G 1990 *Anales Fis.* B **86** 181

[23] Kaptás D, Kemény T, Kiss L F, Gránásy L, Balogh J and Vincze I 1993 *J. Non-Cryst. Solids* **156–8** 336
Vincze I, Kaptás D, Kemèny T, Kiss L F and Balogh J 1984 *Phys. Rev. Lett.* **73** 496
[24] Kaul S N and Siruguri V 1992 *J. Phys.: Condens. Matter* **4** 505
[25] Kaul S N and Babu P D 1992 *Phys. Rev.* B **45** 295
[26] Kaul S N and Mohan Ch V 1992 *J. Appl. Phys.* **71** 6090
[27] Siruguri V and Kaul S N 1996 *J. Phys.: Condens. Matter* **8** 4545
[28] Siruguri V and Kaul S N 1996 *J. Phys.: Condens. Matter* **8** 4567
[29] Obi Y, Wang L C, Motsay R, Onn D G and Nose M 1982 *J. Appl. Phys.* **53** 2304
[30] Mohan Ch V, Babu P D, Sambasiva Rao M, Lucinski T and Kaul S N 1993 *Proc. Int. Conf. on Disordered Materials* ed S K Srivastava (Allahabad: Poonam) p 158
[31] Babu P D, Kaul S N, Fernández Barquin L and Gómez Sal J C 1995 *J. Magn. Magn. Mater.* **140–4** 295
Babu P D, Kaul S N, Fernández Barquin L, Gómez Sal J C, Kettler W H and Rosenberg M 1997 *Phys. Rev.* B at press
[32] Fukamichi K and Gambino R J 1981 *IEEE Trans. Magn.* **17** 3059
[33] Fukamichi K, Hiroyoshi H, Kaneko T, Masunoto T and Shirakawa K 1982 *J. Appl. Phys.* **53** 8107
[34] Liou S H and Chien C L 1984 *J. Appl. Phys.* **55** 1820
[35] Spano M L and Bhagat S M 1981 *J. Magn. Magn. Mater.* **24** 143
[36] Webb D J and Bhagat S M 1984 *J. Magn. Magn. Mater.* **42** 109
[37] Bhagat S M, Webb D J and Manheimer M A 1985 *J. Magn. Magn. Mater.* **53** 209
[38] Continentino M A 1983 *J. Phys. C: Solid State Phys.* **16** L17; 1983 *Phys. Rev.* B **27** 4351
[39] Kaul S N 1980 *Solid State Commun.* **36** 279
[40] Kaul S N 1984 *IEEE Trans. Magn.* **20** 1290
[41] Kaul S N 1985 *J. Magn. Magn. Mater.* **53** 5
[42] Hasegawa R 1975 *Proc. 21st Annual Conf. on Magnetism and Magnetic Materials* ed J J Becker, G H Lander and J J Rhyne (New York: American Institute of Physics) p 216
[43] Hasegawa R, O'Handley R C and Mendelsohn L T 1976 *Proc. 1st Joint MMM–Intermag Conf* ed J J Becker and G H Lander (New York: American Institute of Physics) p 298
[44] Luborsky F E and Walter J L 1972 *IEEE Trans. Magn.* **13** 1635
[45] Takahashi M and Kim E O 1978 *Japan. J. Appl. Phys.* **16** 206
[46] Luborsky F E 1980 *Ferromagnetic Materials* vol 1, ed E P Wohlfarth (Amsterdam: North-Holland) p 451
[47] Fujimori H 1983 *Amorphous Metallic Alloys* ed F E Luborsky (London: Butterworth) p 300
[48] Kaul S N and Babu P D 1992 *J. Phys.: Condens. Matter* **4** 6429